Enhanced Regional Ocean Ensemble Data Assimilation Through Atmospheric Coupling in the SKRIPS Model

Rui Sun[1], Sivareddy Sanikommu[2], Aneesh C. Subramanian[3], Matthew R. Mazloff[1], Bruce D. Cornuelle[1], Ganesh Gopalakrishnan[1], Arthur J. Miller[1], Ibrahim Hoteit[3]

[1]Scripps Institution of Oceanography, California, USA
[2]Physical Sciences and Engineering Division, King Abdullah University of Science and Technology (KAUST), Thuwal, Saudi Arabia
[3]Department of Atmospheric and Oceanic Sciences, University of Colorado Boulder, Colorado, USA

Key Points:

- We implement an ocean ensemble data assimilation system using the SKRIPS ocean–atmosphere coupled model for the Red Sea region.
- The diversity of the atmospheric forcing is an important part of ensemble spread in the ocean model.
- A downscaled ensemble generated by the coupled model performs as well or better than an ocean model ensemble generated with ECMWF ensemble forcing.

Corresponding author: Rui Sun, `rus043@ucsd.edu`

Abstract

We investigate the impact of ocean data assimilation using the Ensemble Adjustment Kalman Filter (EAKF) from the Data Assimilation Research Testbed (DART) on the oceanic and atmospheric states of the Red Sea. Our study extends the ocean data assimilation experiment performed by Sanikommu et al. (2020) by utilizing the SKRIPS model coupling the MITgcm ocean model and the Weather Research and Forecasting (WRF) atmosphere model. Using a 50-member ensemble, we assimilate satellite-derived sea surface temperature and height and in-situ temperature and salinity profiles every three days for one year, starting January 01 2011. Atmospheric data are not assimilated in the experiments. To improve the ensemble realism, perturbations are added to the WRF model using several physics options and the stochastic kinetic energy backscatter (SKEB) scheme. Compared with the control experiments using uncoupled MITgcm with ECMWF ensemble forcing, the EAKF ensemble mean oceanic states from the coupled model are better or insignificantly worse (root-mean-square errors are 30% to -2% smaller), especially when the atmospheric model uncertainties are accounted for with stochastic perturbations. We hypothesize that the ensemble spreads of the air–sea fluxes are better represented in the downscaled WRF ensembles when uncertainties are well accounted for, leading to improved representation of the ensemble oceanic states in EAKF. Although the feedback from ocean to atmosphere is included in this two-way regional coupled configuration, we find no significant effect of ocean data assimilation on the ensemble mean latent heat flux and 10-m wind speed over the Red Sea. This suggests that the improved skill using the coupled model is not from the two-way coupling, but from downscaling the ensemble atmospheric forcings (one-way coupled) to drive the ocean model.

Plain Language Summary

We investigate how combining ocean information accounting for weather processes can help us better understand and predict the ocean–atmospheric state of the Red Sea. We use a coupled ocean and atmosphere model to assimilate satellite and ship-based ocean observations. We assess the performance of the assimilation system using fifty different realizations of the atmospheric state and found that it improves the prediction of oceanic state compared to using the ocean model alone for assimilation and prediction. This success is because the combined ocean–atmosphere model provides a broader range of possible ocean conditions. We also look at how incorporating ocean observation information may potentially impact weather forecasts in the coupled model.

1 Introduction

Numerical models have been used to analyze and predict ocean states for decades. Realistically configured numerical models can simulate oceanic conditions that are generally consistent with observations, but there can be substantial differences when comparing with observations at specific times and locations (Edwards et al., 2015). Even with a perfect model, the differences can result from uncertainties of initial conditions, perturbations, parameterizations, and forcings. Because of this, data assimilation (DA) is used to constrain the model solutions using observational data, including observation uncertainty and model representational error (Edwards et al., 2015).

The Ensemble Kalman Filter (hereafter EnKF) provides an efficient framework for ocean data assimilation (Evensen, 1994). It has gained popularity because of its simple conceptual formulation and relative ease of implementation, requiring no derivation of tangent linear or adjoint models, with only forward model integration in time (Evensen, 2003). Furthermore, its computational requirements scale with ensemble size, and so can be affordable and comparable with other popular sophisticated assimilation methods (Evensen, 2003). EnKF based data assimilation systems have been developed for many applications. For example, Evensen and Van Leeuwen (1996) assimilated altimeter data in the

Agulhas region using a quasi-geostrophic model; Sakov et al. (2012) and Hoteit et al. (2013) respectively produced realistic estimates of the ocean circulation in the North Atlantic and the Gulf of Mexico; Sanikommu et al. (2020) investigated the impact of atmospheric forcing and model physics perturbations using an Ensemble Adjustment Kalman Filter (EAKF). In addition to ocean data assimilation, EnKF is used for operational atmospheric assimilation at the Canadian Meteorological Centre (Houtekamer et al., 2005) among many other applications (e.g., Lawson & Hansen, 2004; Leeuwenburgh et al., 2005; Bannister, 2017).

A major component of EnKF data assimilation systems is the background error covariance estimated from the ensembles (Bannister, 2008a, 2008b; Song et al., 2010). EnKFs can suffer from the collapse of the ensemble spread, which unrealistically reduces the background error covariance in the data assimilation system (e.g., J. Anderson & Anderson, 1999; Hoteit et al., 2002). This is often mitigated using covariance inflation techniques to increase the ensemble spread to better describe the background covariance (J. Anderson & Anderson, 1999; Hoteit et al., 2002; F. Zhang et al., 2004; Whitaker & Hamill, 2012; Luo & Hoteit, 2012). A more representative approach is to account directly for uncertainties in the model, such as the forcing and boundary conditions. Diverse high-resolution forcings that represent the uncertainty of the atmosphere are indeed desirable for ocean ensemble data assimilation system. Many studies have demonstrated improved forecasts and analyses when driving ensemble ocean data assimilation systems with perturbed atmospheric forcing (Lisæter et al., 2003; Evensen, 2004; Wan et al., 2008; Shu et al., 2011; Sakov et al., 2012; Karspeck et al., 2013; Penny et al., 2015; Sanikommu et al., 2017, 2019). Others investigated the perturbed model physics (Sandery et al., 2014; Brankart et al., 2015; Lima et al., 2019), or combined the perturbations of atmospheric forcing and model physics (Vandenbulcke & Barth, 2015; K. M. Kwon et al., 2016; Sanikommu et al., 2020). A recent study by Sanikommu et al. (2020) performed a detailed analysis of the impacts of model physics perturbations and atmospheric forcing on a high-resolution regional ocean DA system. The DA experiments improved the forecasts of oceanic states by using multiple oceanic model physics and ensemble atmospheric forcing now available from operational weather systems.

Our study takes a step forward toward a fully coupled ocean–atmospheric data assimilation system, with application to the Red Sea region. A regional assimilation system is crucial for improving forecasts in the Red Sea due to its unique characteristics in terms of both oceanic and atmospheric conditions (Hoteit et al., 2021). The region is prone to dust and sandstorms, particularly during the transitional seasons of spring and autumn, originating from nearby deserts like the Sahara. These storms significantly reduce visibility and impact air quality (Prakash et al., 2014). The Red Sea also experiences frequent temperature inversions, especially in winter, which affect temperature profiles, pollutant dispersal, and vertical mixing of air masses. The region is influenced by two primary wind patterns: the Southwest Monsoon, bringing humid air and thunderstorms, and the Northwest Monsoon, bringing drier air (Langodan et al., 2017). A sea breeze often develops during the day, cooling coastal areas (Davis et al., 2019). The Red Sea warm surface waters contribute to high levels of water vapor, impacting local weather conditions and precipitation. The local atmospheric features vary significantly with seasons, weather patterns, and local geography (Dasari et al., n.d.). The Red Sea holds economic importance and plays a vital role in international trade. Further, the Red Sea circulation plays a dominant role in modifying the salinity budgets of the western Indian Ocean. Global reanalysis often fails to capture the Red Sea circulation features accurately due to coarse resolutions and limited observations (Sanikommu et al., 2023a). Developing a high-resolution regional reanalysis using local observations and coupled ocean–atmospheric data assimilation system would greatly enhance the forecasts in the Red Sea, and this is important for many applications in this unique region.

In this context, we implement a new ensemble DA system for the Red Sea using the Scripps–KAUST Regional Integrated Prediction System (SKRIPS, Sun et al., 2019, 2023) and the Data Assimilation Research Testbed (DART, J. Anderson et al., 2009). This work is an extension of previous DA efforts for the Red Sea (Toye et al., 2017; Sanikommu et al., 2020, 2023b), replacing the uncoupled ocean model with the SKRIPS coupled model (Sun et al., 2019, 2023). Here we assimilate only oceanic observations using the DART–EAKF system and investigate the estimated oceanic and atmospheric states of the Red Sea regional coupled model, using different options to perturb the physics of the atmosphere model. We evaluate the performance of the coupled model in forecasting the oceanic states, the impact of atmospheric model physics options on the coupled model, and the feedback of the ocean data assimilation to the atmospheric model. Although we only assimilate ocean observations in this work, the present study is a step toward developing a weakly coupled DA system and operational analysis and forecasting system for the Red Sea. Because the random atmospheric states are generated by perturbing the model physics when using a coupled model, there is less need to generate large ensembles of atmospheric forcings (Sanikommu et al., 2023a), enhancing the robustness of the DA system.

The rest of the manuscript is organized as follows. We first introduce the ensemble DA system and its implementation in Section 2. The results of the DA experiments are presented and discussed in Section 3. The final section outlines the main findings and concludes this work.

2 Implementations and Experimental Design

2.1 The Data Assimilation Framework

We use the SKRIPS model (Sun et al., 2019) for the coupled simulation: the oceanic model component is the MIT general circulation model (MITgcm, Marshall et al., 1997; Campin et al., 2019) and the atmospheric model component is the Weather Research and Forecasting (WRF) model (Skamarock et al., 2019). The Earth System Modeling Framework (ESMF, Hill et al., 2004) and the National United Operational Prediction Capability (NUOPC) layer are used to handle the coupling between MITgcm and WRF. The schematic diagram of the DART–SKRIPS framework and the domain used in the experiment are shown in Fig. 1. The ocean data are assimilated using EAKF available from the DART–MITgcm package (Hoteit et al., 2013, 2015), aiming to evaluate their impact on the ocean and atmosphere states in the coupled system. The ROCOTO workflow (Harrop et al., 2017) is used for the management of the pre- and post-processing scripts in the developed DART–SKRIPS framework.

The coupled model is also described in the diagram shown in Fig. 1. In the coupling process, MITgcm sends sea surface temperature (SST) and ocean surface velocity to WRF; WRF sends air-sea flux and surface atmospheric fields to MITgcm, including (1) net surface longwave and shortwave radiative fluxes, (2) surface latent and sensible heat fluxes, (3) 10-m wind speed, (4) precipitation, and (5) evaporation. The MITgcm model uses the surface atmospheric variables to prescribe surface forcing, including (1) total net surface heat flux, (2) surface wind stress, and (3) freshwater flux. The total net surface heat flux is computed by adding surface latent heat flux, sensible heat flux, net shortwave radiation flux, and net longwave radiation flux. The surface latent and sensible heat fluxes are computed using the COARE 3.0 bulk algorithm in WRF (Fairall et al., 2003).

2.2 Experimental Design

To study the impact of ocean data assimilation on the oceanic and atmospheric states, we perform a series of 50-member ensemble DA experiments using coupled and uncoupled models starting from January 01 2011, assimilating the observational data every 3

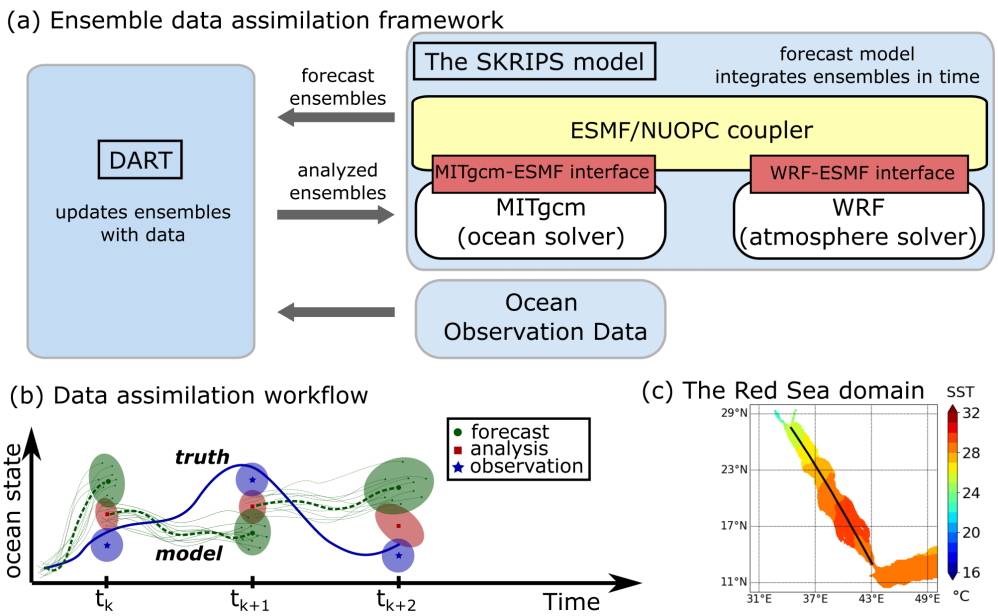

Figure 1. The schematic description of the DART–SKRIPS data assimilation system. Panel (a) indicates the DART–SKRIPS framework: the blue blocks denote the SKRIPS model, DART, and ocean observations; the yellow block is the ESMF/NUOPC coupler; the white blocks are the ocean and atmosphere components; the red blocks are the implemented MITgcm–ESMF and WRF–ESMF interfaces. The arrows indicate the information exchange between DART and SKRIPS. Panel (b) shows the workflow at three time steps: the thick solid line indicates the evolution of the "truth"; the dashed line indicates the ensemble averaged forecast; the thin solid lines indicate the evolution of the ensemble members; the red dots indicate the analysis; the shaded areas indicate the error covariance; t_k, t_{k+1}, and t_{k+2} indicate three steps when observational data are assimilated. Panel (c) shows the domain of the coupled model, with the black line indicating the centerline of the Red Sea.

days. For the coupled model experiments, the ocean and atmosphere models are nested in GLORYS and ERA5 reanalyses, respectively. For the uncoupled model experiments, the ocean model is also nested in GLORYS, but driven by ECMWF derived atmospheric forcing. Further details on the initial and boundary conditions will be discussed in the latter sections. The same setup is used for the ocean model, but different options are used for the atmosphere in the 50-member ensemble DA experiments:

1. OCN.daO uses only the ocean model forced by the ECMWF ensemble mean.
2. OCN.daF uses only the ocean model forced by the 50-member ECMWF ensembles.
3. CPL.daO uses the coupled model with no perturbations to the atmosphere.
4. CPL.daS uses the coupled model with stochastic forcings in the atmospheric model.
5. CPL.daP uses the coupled model with perturbed physics options in the atmospheric model (e.g., microphysics, convection, and planetary boundary layer).
6. CPL.daSP uses the coupled model with stochastic forcings and perturbed atmosphere physics options.

OCN.daO and OCN.daF follow the experiments using the ocean-only models in Sanikommu et al. (2020), but without inflation to investigate the changes using the coupled model. They also serve as benchmarks to evaluate the performance of the coupled experiments. In the coupled DA experiment CPL.daO, although we did not perturb the atmospheric

model physics, the randomness of the atmospheric forcing is from the feedback of different ocean states. Different random seeds are used for the stochastic model in CPL.daS and CPL.daSP from 1 to 50. The coupled DA experiments OCN.daS, OCN.daP, and OCN.daSP are conducted to assess the effect of different strategies of the atmospheric forcings, and thus we did not assimilate the atmospheric observational data in our experiments. Although the ocean feedback is important in the coupled model, we did not perform DA experiments driven by the atmospheric forcings from stand-alone WRF models because it is out of the scope of our work.

2.3 The Forward Models

The initial conditions, boundary conditions, and forcings are outlined in Table 1. The MITgcm initial conditions are obtained from a spin-up run as described in Sanikommu et al. (2020), with randomly selecting 50 ocean states corresponding to ±15 days from the initial time. The boundary conditions for the ocean are updated by linearly interpolating between the daily data from Global Ocean Reanalysis and Simulation (GLORYS, Jean-Michel et al., 2021). For the uncoupled experiments, the atmospheric forcings are from the ECMWF atmospheric ensemble from The Observing System Research and Predictability Experiment Interactive Grand Global Ensemble project (TIGGE, Bougeault et al., 2010), with full details available in Buizza (2014). We combined the fields of the 00 and 12 UTC TIGGE initial conditions and 06 and 18 UTC forecasts as 6-hourly forcing for our ocean ensemble assimilation runs. For OCN.daO, we forced the model with the ensemble mean of the atmospheric forcings; for OCN.daF, we forced the model with the ECMWF 50-member ensembles. In the coupled experiments, ERA5 provides the initial and boundary conditions for the atmosphere model, with the atmospheric boundary conditions updated by linearly interpolating between the 6-hourly fields. Spectral nudging is not used in the DA experiments because (1) nudging may constrain the high frequency internal variability of the atmosphere model and (2) the domain size is comparable with wavelengths typically used in the spectral nudging simulations (Liu et al., 2012).

We choose the latitude–longitude (cylindrical equidistant) map projection to generate the grids for MITgcm and WRF. The domains for both models extend from 10°N to 30°N and from 30°E to 50°E. In the ocean model, the horizontal grid has 500×500 (lat×long) cells and the spacing is about 4 km; in the atmospheric model, the horizontal grid has 125×125 (lat×long) cells and the spacing is about 16 km. There are 40 sigma layers in the atmospheric model (top pressure is 50 hPa) and 50 z-layers in the ocean model ($\mathrm{d}z = 4$ m at the top). The time step of the oceanic model is 200 seconds; the time step of the atmospheric model is 25 seconds; the coupling interval is 200 seconds.

2.4 Model Perturbations

For the oceanic simulations in all DA experiments, we use various physical parameterization schemes to account for the effects of unresolved scales of motion as proposed by Sanikommu et al. (2020), summarized in Table 2. Three different categories of model physics are selected: horizontal viscosity, vertical mixing, and horizontal diffusion. We include three different horizontal viscosity schemes: the simple harmonic scheme, the simple biharmonic of Holland (1978), and the Smagorinsky/Leith scheme (Smagorinsky et al., 1993; Griffies & Hallberg, 2000) with the coefficients suggested in the literature (Leith, 1996; Griffies & Hallberg, 2000). For vertical mixing, four different schemes are included: the nonlocal K-Profile Parameterization (KPP) scheme (W. G. Large et al., 1994), the PP81 scheme (Pacanowski & Philander, 1981), the MY82 scheme (Mellor & Yamada, 1982), and the GGL90 scheme (Gaspar et al., 1990). For the horizontal diffusion, we use implicit diffusion, simple-explicit harmonic diffusion, and three different flavors of Gent-McWilliams/Redi subgrid-scale eddy parameterization schemes (hereafter GMREDI, Gent & Mcwilliams, 1990; Gent et al., 1995; Redi, 1982): the GMREDI clipping scheme of Cox

(1987), the GMREDI-dm95 tapering scheme of Danabasoglu and McWilliams (1995), and the GMREDI-ldd92 tapering scheme of W. Large et al. (1997). Table 2 lists the coefficients used in these schemes.

We also perturb the physics options in WRF to parameterize microphysics, convection, and planetary boundary layer (PBL), summarized in Table 3. For the microphysics we use the Morrison 2–moment scheme (Morrison et al., 2009), the Purdue-Lin scheme (Chen & Sun, 2002), the Thompson scheme (Thompson et al., 2008), the WRF single moment 6-class scheme (Hong & Lim, 2006), and the WRF double moment 6-class scheme (Lim & Hong, 2010). For the cumulus convection, we use the Kain–Fritsch scheme (Kain, 2004), the Betts–Miller–Janjic scheme (Janjić, 1994), the Grell–Freitas Ensemble scheme (Grell & Freitas, 2014), the new Tiedtke scheme (C. Zhang & Wang, 2017), and the simplified Arakawa–Schubert scheme (Y. C. Kwon & Hong, 2017). For the planetary boundary layer, we use the Mellor–Yamada Nakanishi Niino scheme (MYNN, Nakanishi & Niino, 2004, 2009), the Yonsei University scheme (Hong et al., 2006), and the Mellor–Yamada–Janjic scheme (Janjić, 1994). The radiation and land surface schemes are not perturbed: the Rapid Radiation Transfer Model for GCMs (RRTMG, Iacono et al., 2008) is used for longwave and shortwave radiation transfer through the atmosphere; the Noah land surface model is used for the land surface processes (Tewari et al., 2004). The physics scheme perturbation is based on the ensemble forecast system of the Center For Western Weather and Water Extremes (CW3E, Oakley et al., 2023). For the experiments without perturbing the atmospheric model (i.e., CPL.daO and CPL.daS), we use Morrison 2–moment scheme, Kain–Fritsch scheme, and MYNN scheme for microphysics, convection, and PBL, respectively.

In addition to perturbing the atmospheric model physics, we used the SKEB scheme (Shutts, 2005; Berner et al., 2009) to account for the unrepresented uncertainties in the model. This scheme adds stochastic, small-amplitude perturbations to the horizontal wind and potential temperature. The default amplitudes of the stochastic perturbations in WRF were used in CPL.daS and CPL.daSP, which were able to provide more reliable ensemble spreads (Berner et al., 2011, 2015).

2.5 Data Used in Assimilation and Validation

We assimilate data from level-4 SST blended daily product available on a $0.25° \times 0.25°$ grid (Reynolds et al., 2007; Banzon et al., 2016), along-track satellite altimeter level-3 sea level anomalies (SLAs; corrected for dynamic atmospheric loading, ocean tide, and long wavelength errors) available from Copernicus Marine Environment Monitoring Service (here after CMEMS-L3, Mertz et al., 2017), and quality controlled in situ glider temperature and salinity profiles from EN4 data (Ingleby & Huddleston, 2007; Good et al., 2013). The in situ temperature and salinity profiles are sparse, and there are only 244 temperature and 110 salinity profiles in the entire year 2011 from the glider in the Red Sea. Errors associated with these observations are assumed uncorrelated, so the observational error covariance matrix is diagonal. The combined observation and representation error variance is determined based on previous DA experiments (Toye et al., 2017; Sanikommu et al., 2020) and accounts for errors due to: measurement devices, omitted processes, unresolved subgrid scale dynamics, and numerical errors in interpolation. Temporally static, partially homogeneous, and depth independent observational error variance values of $(0.5°\mathrm{C})^2$, $(0.04\ \mathrm{m})^2$, $(0.5°\mathrm{C})^2$, and $(0.3\ \mathrm{psu})^2$ are then used for satellite SST, satellite along-track SLA, in situ temperature and salinity, respectively. A cutoff radius of about 300 km was imposed to localize the impact the observations in the horizontal directly (not in the vertical) as a way to mitigate spurious correlations.

For validation, we evaluate the daily averaged ocean forecasts and analyses as resulting from the DA experiments. We first use the assimilated data to examine the time series of innovations and residuals. In addition to the assimilated data, independent ob-

Table 1. The computational domain, WRF physics schemes, initial condition, boundary condition, and forcing terms used in the present simulations.

	OCN Experiments	CPL Experiments
Model region	10°N to 30°N; 30°E to 50°E	
Grid size	500×500	500×500 for ocean 125×125 for atmosphere
Grid spacing	0.04° × 0.04°	0.04° × 0.04° for ocean 0.16° × 0.16° for atmosphere
Microphysics scheme	Not necessary	Various (see Table 3)
Convection scheme		Various (see Table 3)
PBL scheme		Various (see Table 3)
Longwave radiation scheme		RRTMG
Shortwave radiation scheme		RRTMG
Land surface scheme		Noah land surface model
Vertical levels	50 (ocean only)	40 (atmosphere) 50 (ocean)
Initial and boundary conditions	GLORYS (ocean only)	ERA5 (atmosphere) GLORYS (ocean)
Atmospheric forcings for oceanic model	From ECMWF TIGGE product	From WRF

Table 2. MITgcm model physics parameterizations in the present study.

Horizontal Viscosity	Vertical Mixing	Horizontal Diffusion
Simple Harmonic (30 m^2/s)	K-Profile Parameterization	Implicit Diffusion
Simple Biharmonic (10^7 m^4/s)	PP81	Explicit Diffusion (100 m^2/s)
SMAGLEITH-Harmonic (30 m^2/s), Smag Coeff 2.5, and Leith Coeff 1.85	MY82	GMREDI-clipping (100 m^2/s)
	GGL90	GMREDI-dm95 (100 m^2/s) GMREDI-ldd92 (100 m^2/s)

Table 3. WRF model physics parameterizations in the present study. The physics options used in the experiments without perturbing the model physics (i.e., CPL.daO and CPL.daS) are highlighted using bold red color.

Microphysics	Convection	Planetary Boundary Layer
Morrison 2-moment	**Kain–Fritsch**	**Mellor–Yamada Nakanishi Niino**
Purdue-Lin	Betts–Miller–Janjic	Yonsei University
Thompson	Grell–Freitas Ensemble	Mellor–Yamada–Janjic
WRF single moment 6-class	New Tiedtke	
WRF double moment 6-class	Simplified Arakawa–Schubert	

servations are used. To analyze the subsurface features, we use 206 profiles of temperature and salinity collected between September 15 to October 08 2011 by a joint Woods Hole Oceanography Institute (WHOI) and King Abdullah University of Science and Technology (KAUST) cruise along the eastern part of the Red Sea, collected with a horizontal spacing of 10 km (Zhai et al., 2015). We also use other satellite products to evaluate the DA results. For SST we select the high-resolution daily averaged level 4 SST product from the Operational Sea Surface Temperature and Sea Ice Analysis (OSTIA, Stark et al., 2007; Donlon et al., 2012) because it is mapped differently with higher resolution. For sea surface height (SSH) we use multimission altimeter merged satellite level 4 gridded absolute dynamic topography (ADT) provided by CMEMS (hereafter CMEMS-L4, Mertz et al., 2017). Compared with the assimilated CMEMS-L3 data, the CMEMS-L4 data is gridded on a 0.25° grid and thus can be used to estimate the errors across the entire Red Sea region. The SSH anomaly from the DA experiments is the instantaneous SSH obtained in the simulations minus the time-averaged SSH from the 15-year MITgcm model in Sanikommu et al. (2020). The SSH anomalies in CMEMS-L3 and CMEMS-L4 are the sea level height above the mean surface based on the long-term averaged observations between 1993 to 2012. Because of the lack of in situ observational data of the atmosphere, we use ERA5 to validate the latent heat fluxes and wind speed simulated by the coupled experiments.

3 Results

The results obtained from the DA experiments are presented in this section. First, we analyze the ensemble spread of the atmospheric forcings and sea surface temperature. Then we examine the ocean states (e.g., SST, SSH, and vertical profiles) to assess the impact of atmospheric forcings in the uncoupled and coupled systems using the validation data. In addition to the ocean states, the air–sea exchanges (e.g., latent heat flux) and surface atmospheric states (e.g., wind speed) are also analyzed to illustrate the feedback from the ocean to the atmosphere due to assimilation. Finally, we discuss the changes in the ocean dynamics from assimilating the observation data.

3.1 Ensemble Spread Analysis

Similarly to the DA experiments in Sanikommu et al. (2020), we hypothesize that the estimated ocean states are improved when uncertainties in various sources are well accounted for. Incorporating uncertainties in the system improves ensemble spreads in the ocean systematically. For instance, Figs. 2 and 3 display the temporal evolution of atmospheric forcing root-mean-square (RMS) spread in the DA experiments, except for OCN.daO which is forced by the ECMWF ensemble mean. The spread in OCN.daF is from the ECMWF ensemble atmospheric forcing; others are from the coupled model outputs. In comparison with OCN.daF, the spread in CPL.daO is smaller by about one order of magnitude because the atmospheric models are not perturbed and the spread of atmosphere is from the ocean perturbations. When the SKEB scheme is applied in CPL.daS and CPL.daSP, the spread of the atmospheric forcing is larger than that in OCN.daF, which in turn increases the SST spread, shown in Fig. 4. The impact of the atmospheric forcings on the ocean states will be detailed in the latter sections.

3.2 Sea Surface Temperature

We analyze the SST obtained in our DA experiments to assess its sensitivity to the atmospheric perturbations. The root-mean-square-errors (RMSEs) between the SST analyses and observations in all DA experiments are shown in Fig. 5 and summarized in Table 4. The best SST forecast and analysis are both from experiment CPL.daSP, when the SKEB scheme is turned on and the WRF physics options are perturbed. The SSTs obtained in the coupled experiments (CPL.daS, CPL.daP, and CPL.daSP; except for the

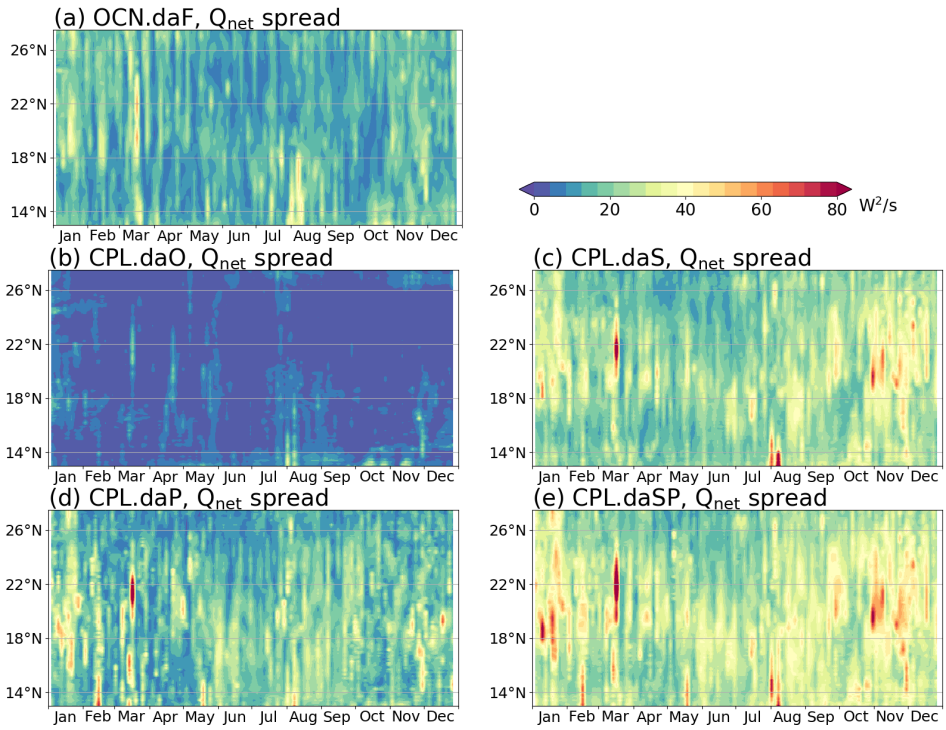

Figure 2. The spatial and temporal evolution of the RMS spread of net surface heat flux Q_{net} along the center line of the Red Sea shown in Fig. 1(c). The Q_{net} is calculated by summing up the latent heat flux, sensible heat flux, net surface shortwave fluxes, and net surface longwave fluxes. Panel (a) shows the spread in the ocean-only experiment driven by ECMWF derived forcing; Panel (b-e) show the spread in the coupled experiments with no perturbations, only SKEB, only perturbed model physics, and SKEB + perturbed model physics, respectively.

benchmark case CPL.daO) are better than that of the uncoupled experiment OCN.daF, with improvements more than twice larger than standard error of the mean SST from CPL.daSP (about 0.015°C, the standard deviation of SST divided by the square-root of the number of ensemble members). Better improvements are obtained when using only the stochastic forcings (CPL.daS) compared with only perturbing the WRF physics (CPL.daP), but this difference is less significant (smaller than 0.015°C). Although the perturbations in the atmospheric forcing are small in CPL.daO (shown in Figs. 2 and 3), the RMSE errors of SST forecasts and analyses are improved compared to the benchmark experiment OCN.daO by 0.156°C and 0.101°C, respectively. This indicates that small perturbations of the atmospheric forcing can improve SST in the DA experiments.

Figure 5 shows that the RMSEs of SST forecasts and analyses increase in summer for the benchmark runs (i.e., OCN.daO and CPL.daO), but RMSEs get smaller when using the coupled model (i.e., CPL.daS, CPLdaP, and CPL.daSP). In this season, the SST has a larger spread in all the experiments, similar to the results shown in Sanikommu et al. (2020), likely because the ocean is more sensitive to heat fluxes when the mixed layer depth is shallower.

In addition to the assimilated data, we validated the SSTs using the OSTIA SST. The RMSEs and correlations are shown in Fig. 6 and summarized in Table. 4. We present the SST correlations to evaluate the forecast of the SST evolution during the year. It can be seen that the SST obtained in CPL.daSP has larger correlations and smaller RMSEs in the north Red Sea, center Red Sea, and Gulf of Aden regions. Compared with the uncoupled experiment OCN.daF, the coupled experiment CPL.daSP has a smaller RMSE by 0.035°C (6.5%, more than twice the standard error). On the other hand, the

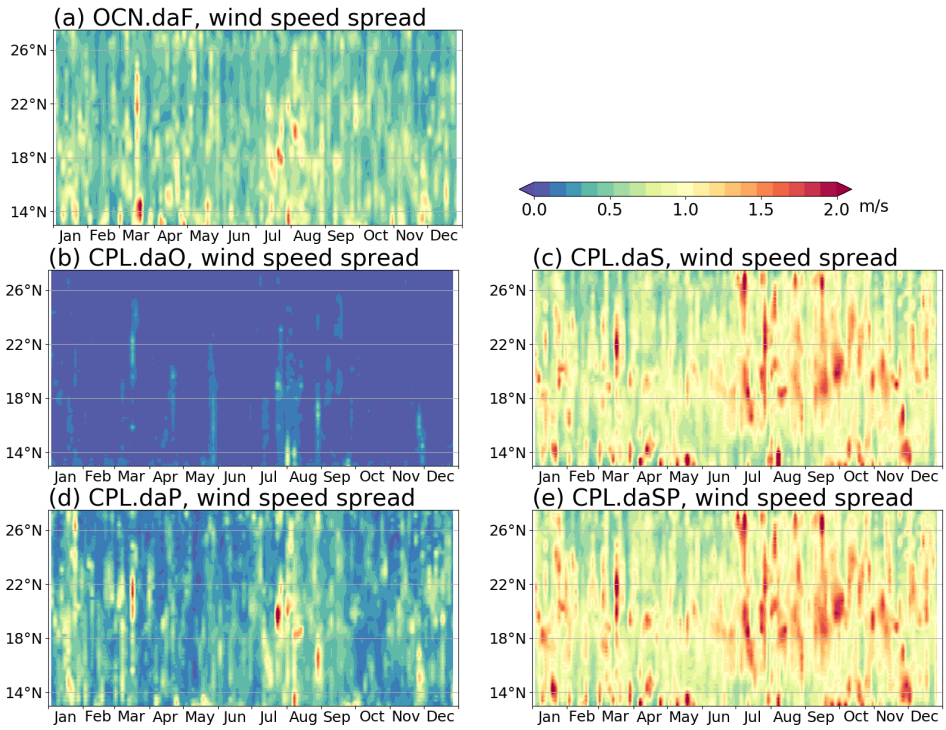

Figure 3. The spatial and temporal evolution of the RMS spread of 10-m wind speed along the center line of the Red Sea shown in Fig. 1(c). Panel (a) shows the spread from the ECMWF derived forcing; Panel (b-e) show the spread in the coupled experiments with no perturbations, only SKEB, only perturbed model physics, and SKEB + perturbed model physics, respectively.

SST analysis obtained in CPL.daSP has a slightly larger RMSE compared to that obtained in CPL.daF, but the differences between OCN.daF, CPL.daS, CPL.daP, and CPL.daSP are within 0.01°C (2%). In addition, the CPL.daSP also has the smallest distance between the forecasts and analyses RMSEs, indicating less "assimilation shock" and more balanced ocean states in the DA experiment.

3.3 Sea Surface Height

The SSH fields as estimated in the DA experiments are presented in Fig. 7 and Table 5. Similar to the SST results, the coupled DA experiments exhibit smaller RMSE and larger spread. The SSH forecast errors in OCN.daF, CPL.daS, CPL.daP, and CPL.daSP are not significantly different. Although CPL.daSP still has the smallest RMSEs, the differences are within 1% and smaller than the standard errors (about 0.001 m). For the SSH analyses, on the other hand, the CPL.daS and CPL.daSP are more significantly improved (RMSEs are smaller by 10% compared with OCN.daF and CPL.daP) when SKEBS are used, suggesting that including the stochastic forcing in model parameters is the key for improvements. Note that the spread of surface wind forcing shown in Fig. 3 is greatly increased when using the stochastic forcing.

The temporal evolution of the SSH is also examined by comparing with CMEMS-L4 data, shown in Fig. 8. Here we only highlight the differences of the SSH analyses because the forecasts are close to each other. Figure. 8 shows that the CPL.daSP experiment has larger correlations and smaller RMSEs in both the Red Sea and the Gulf of Aden regions. Similar to the results shown in Fig. 7, when using the stochastic forcings in WRF, CPL.daS and CPL.daSP outperform the uncoupled model OCN.daF (see Table 5).

Table 4. SST obtained in the DA experiments against the validation data. We highlighted the best forecast/analysis using red, but the pink color is used when the differences between uncoupled and coupled experiments are insignificant (when the RMSE difference is smaller than 5% or the standard error).

	OCN.daO	OCN.daF	CPL.daO	CPL.daS	CPL.daP	CPL.daSP
Against assimilated data						
SST forecast RMSE	0.656	0.486	0.500	0.419	0.426	0.403
SST analysis RMSE	0.475	0.341	0.374	0.281	0.294	0.262
Against OSTIA SST						
SST forecast RMSE	0.650	0.574	0.610	0.560	0.551	0.539
SST analysis RMSE	0.486	0.463	0.484	0.468	0.472	0.469
SST forecast correlation	0.9580	0.9623	0.9573	0.9637	0.9628	0.9649
SST analysis correlation	0.9786	0.9805	0.9773	0.9800	0.9788	0.9791
SST forecast spread	0.078	0.080	0.077	0.098	0.095	0.108
SST analysis spread	0.046	0.052	0.048	0.059	0.055	0.062

Table 5. Summary of SSH against the validation data. We highlighted the best forecast/analysis using red, but the pink color is used when the differences between coupled and coupled experiments are insignificant (when the RMSE difference is smaller than 5% or the standard error).

	OCN.daO	OCN.daF	CPL.daO	CPL.daS	CPL.daP	CPL.daSP
Against assimilated data						
SSH forecast RMSE	0.0646	0.0626	0.0650	0.0624	0.0626	0.0620
SSH analysis RMSE	0.0580	0.0495	0.0578	0.0446	0.0522	0.0433
Against CMEMS-L4 SSH						
SSH forecast RMSE	0.0513	0.0486	0.0513	0.0483	0.0494	0.0482
SSH analysis RMSE	0.0461	0.0390	0.0455	0.0356	0.0409	0.0350
SSH forecast correlation	0.9121	0.9197	0.9109	0.9197	0.9168	0.9204
SSH analysis correlation	0.9314	0.9493	0.0320	0.9578	0.9439	0.9590
SSH forecast spread	0.0034	0.0056	0.0036	0.0073	0.0048	0.0076
SSH analysis spread	0.0023	0.0038	0.0024	0.0046	0.0032	0.0047

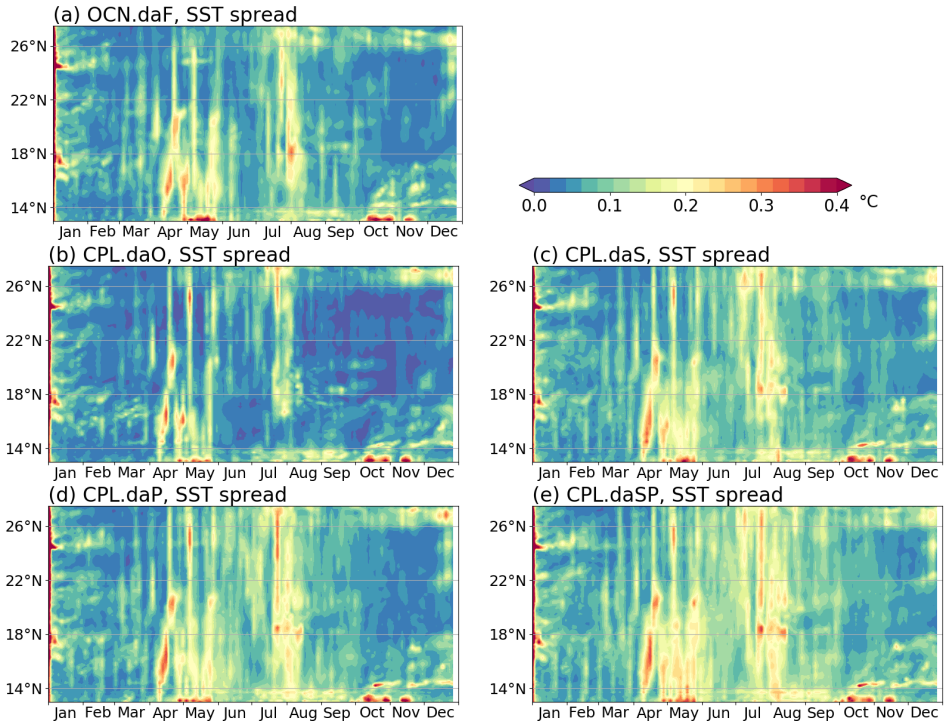

Figure 4. The spatial and temporal evolution of the RMS spread of Sea Surface Temperature along the center line of the Red Sea shown in Fig. 1(c). Panel (a) shows the spread in the ocean-only experiment driven by ECMWF derived forcing; Panel (b-e) show the spread in the coupled experiments with no perturbations, only SKEB, only perturbed model physics, and SKEB + perturbed model physics, respectively.

3.4 Temperature and Salinity Profiles

The subsurface features of the ocean are validated against independent (i.e. not assimilated) CTD observations of temperature and salinity from the WHOI/KAUST summer cruise in the Red Sea between September 15 and October 08 2011. The difference between daily averaged forecasts and observations is shown in Figs. 9 and 10. More than 2 degree and 0.8 psu differences are found for temperature and salinity profiles in the thermocline between 50–100 m. For the temperature profiles, the RMSE in CPL.daSP (0.361°C) is smaller than OCN.daO (0.408°C) by about 10%, especially near the ocean surface, but within 2% difference compared to OCN.daF, CPL.daO, and CPL.daS. For the salinity profiles, the forecast RMSE of CPL.daSP (0.082 psu) is smaller than the benchmark experiment OCN.daO by about 30%. It is noted that CPL.daP has the smallest RMSE for temperature (0.344°C), but its salinity RMSE is significantly larger (0.122 psu) than CPL.daSP. Compared with the ocean-only experiment OCN.daF, the RMSEs in CPL.daS and CPL.daSP are not significantly different (within 1% or 2%). Although the coupled experiment is no better than the best uncoupled experiment OCN.daF, the results indicate the stochastic schemes in WRF are crucial for producing better forecasts of the ocean profiles.

3.5 Feedback to the Atmosphere

To assess the impact of ocean data assimilation on the surface of the atmosphere, we compare the latent heat fluxes and 10-m wind speed obtained in the DA experiments. This analysis informs feedback to the heat and momentum fluxes. We consider ERA5 as reference and present the RMSEs of latent heat fluxes and 10-m wind speed in Fig. 11. Here we only compare the data on the centerline of the Red Sea to highlight ocean re-

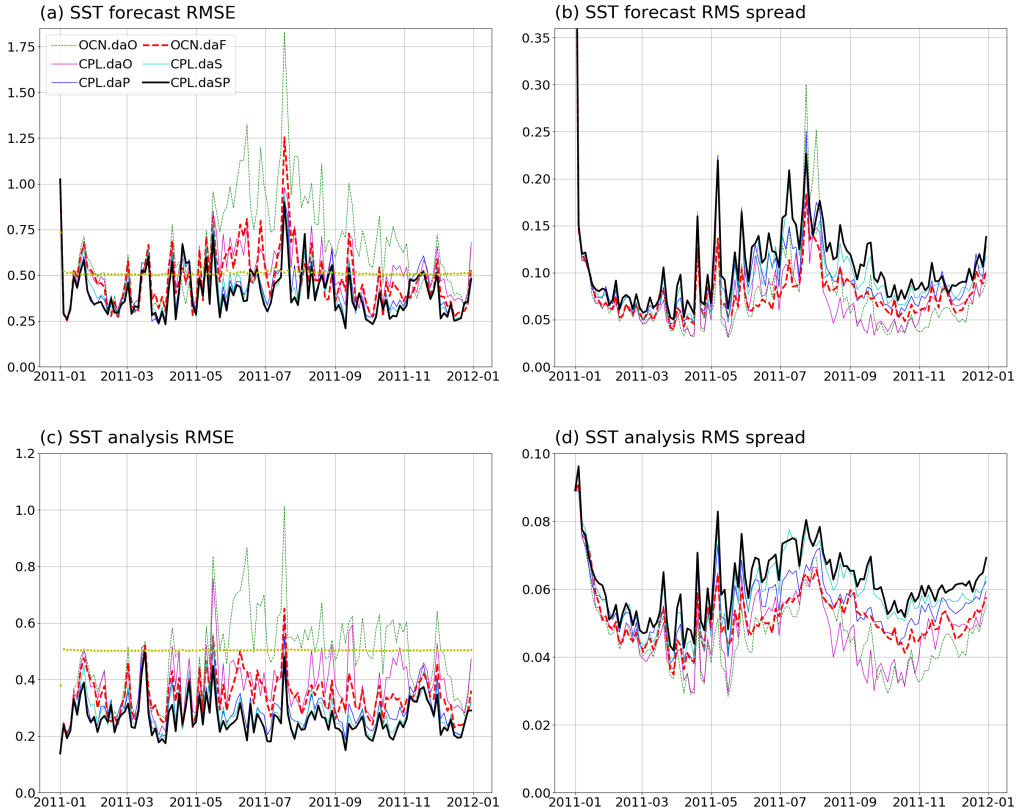

Figure 5. Time history of SST RMSEs and spreads during the data assimilation experiment. Panels (a) and (c) show the RMSEs of the forecasts and analyses against the assimilated data; Panels (b) and (d) show the spread of SST in the forecasts and analyses. The yellow dots in Panels (a) and (c) indicate the total uncertainty (square root of the sum of ensemble variance and observational variance $(0.5°\mathrm{C})^2$) of CPL.daSP.

gions. It can be seen that the RMSEs do not grow significantly with time, showing the capability of the coupled system for the 1-year DA experiments. We hypothesize this is because the atmospheric states are constrained by the boundary conditions for this relatively small domain. Compared with the benchmark case CPL.daO, the RMSEs of the latent heat flux and 10-m wind speed obtained from CPL.daSP are smaller by about 4%, but the RMSE differences are smaller than the standard error, implying the improved ocean states may not significantly impact the atmospheric states. Because of the small differences in the surface atmosphere, this indicates that for the Red Sea region, the skill of the coupled model is not from the two-way coupling, but from the atmospheric forcings in the downscaled WRF ensembles (one-way coupled) to drive the ocean model.

3.6 Vertical Current Velocity

Toye et al. (2017) argued that the dynamical balances (or assimilation shock) in the oceanic model from the EAKF increments increase the spread of the Red Sea forecasts. The imbalances are also reported in other EAKF assimilation experiments (L. A. Anderson et al., 2000; Hoteit et al., 2010; Park et al., 2018). Here, we investigate the dynamical balances in our experiments by comparing the standard deviation of $|w|$ obtained in the DA experiments with the "free" run without assimilating observation data in Fig. 12. The results show that the spreads of $|w|$ in all DA experiments are larger than the "free" run for the Red Sea region, but there are no significant changes in $|w|$ spread when the

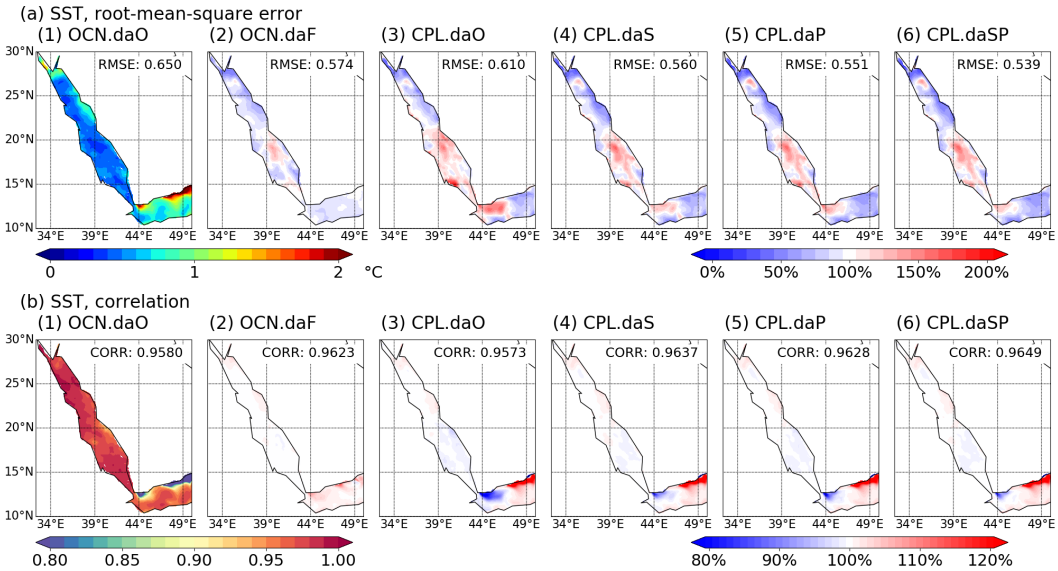

Figure 6. SST RMSEs and correlations obtained in the DA experiments validated against OSTIA. Panels (a) and (b) show the RMSE and correlation of the "forecast" SST. The contours in column 1 indicate the comparison with OSTIA data; columns 2-5 are normalized by the reference OCN.daO in column 1 to highlight differences, showing the ratios in percentage.

coupled model is used in comparison with ocean-only model experiments, indicating no significant dynamical imbalances.

4 Summary and Conclusions

This work implemented a data assimilation framework based on the regional coupled model SKRIPS and DART. Using the EAKF in DART, we investigate the impact of ocean data assimilation on the oceanic and atmospheric states of the Red Sea. The coupled system assimilates satellite-based sea surface temperature and height and in situ temperature and salinity glider profiles every 3 days for 1 year starting from January 01, 2011.

To assess the performance of the ensemble forecasts and examine the generated ocean states, we ran a series of experiments using different perturbation schemes. The assimilation results of the coupled experiments are compared with the uncoupled ones forced by ECMWF-derived surface forcing, revealing that the coupled experiments give greater spread in the ensembles of ocean states, with the spread continuing to increase when using the stochastic kinetic energy backscatter (SKEB) scheme. Compared with the assimilated data, the coupled experiments result in a more skillful SST and SSH ensemble mean forecast. The SST forecasts and SSH analyses in coupled models are also better than uncoupled ones when compared with the independent observational data, but the RMSEs of SST analyses and SSH forecasts are insignificantly different.

We further compared the DA experiment results with the independent cruise observation data of temperature and temperature profiles. The comparison shows large variations in the temperature profiles because of the challenge in modeling the thermocline layer and the lack of in situ data. The RMSEs from the coupled DA experiments with perturbations of the atmospheric model are comparable to the uncoupled model driven by ECMWF-derived ensemble forcing, and both are better than the benchmark experiments with small spreads in atmospheric forcings. To investigate the feedback from the

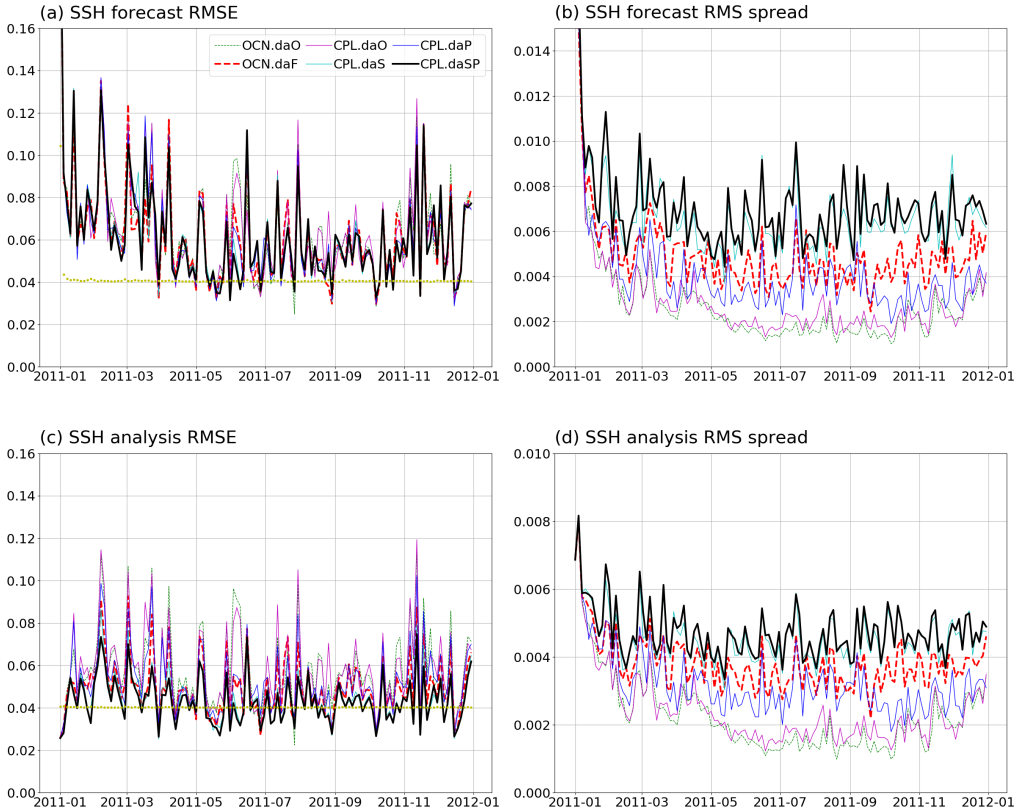

Figure 7. Evolution of the SSH RMSEs and spreads during the data assimilation experiment. Panels (a-b) show the RMSEs of the forecasts and analyses against the assimilated data; Panels (c-d) show the RMS spread of SSH in the forecasts and analyses. The yellow dots in Panels (a) and (c) indicate the total uncertainty (square root of the sum of ensemble variance and observational variance $(0.04\ \mathrm{m})^2$) of CPL.daSP.

ocean, we validated the latent heat flux and 10 m winds in all coupled experiments using ERA5 data, but no significant difference is observed.

This study demonstrates that our Red Sea DA system using two-way coupled model with WRF performs better or equal to an uncoupled model driven by ECMWF-derived ensemble surface forcing, showing a promising approach for forecasting the oceanic states or producing ocean analysis data. The dynamical imbalances in the coupled model are also not significantly different from the uncoupled model. The DA system implemented here explores the utility of a coupled DA system and studies of the ocean–atmosphere interactions using the analysis data.

Acknowledgments

We gratefully acknowledge the research funding (grant number: OSR-2022-NCM-4829.5) from KAUST (King Abdullah University of Science and Technology). We also appreciate the computational resources of the supercomputer Shaheen II and the assistance provided by KAUST Supercomputer Laboratory. RS and ACS were supported by ONR ASTRAL research initiative (N00014-23-1-2092). ACS was supported by NOAA Grant NA18OAR4310405 and ONR MISOBOB research initiative (N00014-17-S-B001). BDC and MRM were supported by NOAA Grant NA21OAR4310257, NA18OAR4310403, and NA22OAR4310597. AJM was partly supported by the National Science Foundation (OCE-

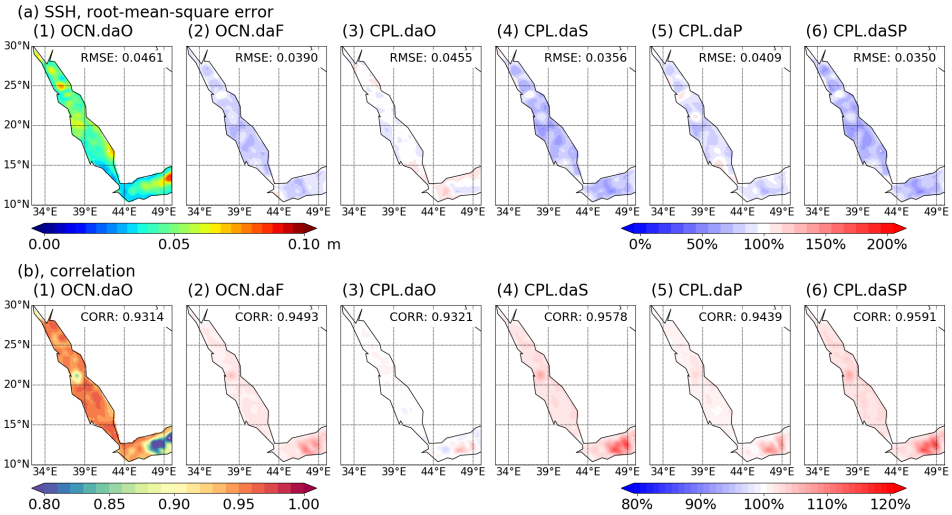

Figure 8. SSH RMSEs and correlations obtained in the DA experiments validated against CMEMS-L4 data. Panels (a) and (b) show the RMSEs and correlations of the SSH analyses. The contours in column 1 indicate the comparison with CMEMS-L4 data; columns 2-5 are normalized by the reference OCN.daO in column 1 to highlight differences, showing the ratios in percentage

2022868). We appreciate Luca Delle Monache, Daniel Steinhoff, and Rachel Weihs for discussing the generation of WRF ensembles.

Data Availability Statement

The coupled model used for the simulations is available at `https://github.com/iurnus/scripps_kaust_model`. The DA experimental results used in the paper are available at https://zenodo.org/records/10408667.

Author contributions statement

All authors conceived the experiments; R.S. implemented the DA system for the coupled models; S.S. implemented the DA system for the uncoupled models and the ROCOTO workflow; R.S. conducted the experiments and plotted the figures; R.S. and S.S. drafted the initial manuscript; all authors discussed the results and revised the manuscript.

Competing Interests

The authors declare no competing interests.

References

Anderson, J., & Anderson, S. (1999). A Monte Carlo implementation of the nonlinear filtering problem to produce ensemble assimilations and forecasts. *Monthly Weather Review*, *127*(12), 2741-2758. doi: 10.1175/1520-0493(1999)127⟨2741:AMCIOT⟩2.0.CO;2

Anderson, J., Hoar, T., Raeder, K., Liu, H., Collins, N., Torn, R., & Avellano, A. (2009). The Data Assimilation Research Testbed: A community facility. *Bulletin of the American Meteorological Society*, *90*(9), 1283–1296.

Anderson, L. A., Robinson, A. R., & Lozano, C. J. (2000). Physical and biological modeling in the Gulf Stream region:: I. Data assimilation methodology. *Deep Sea Research Part I: Oceanographic Research Papers*, *47*(10), 1787–1827.

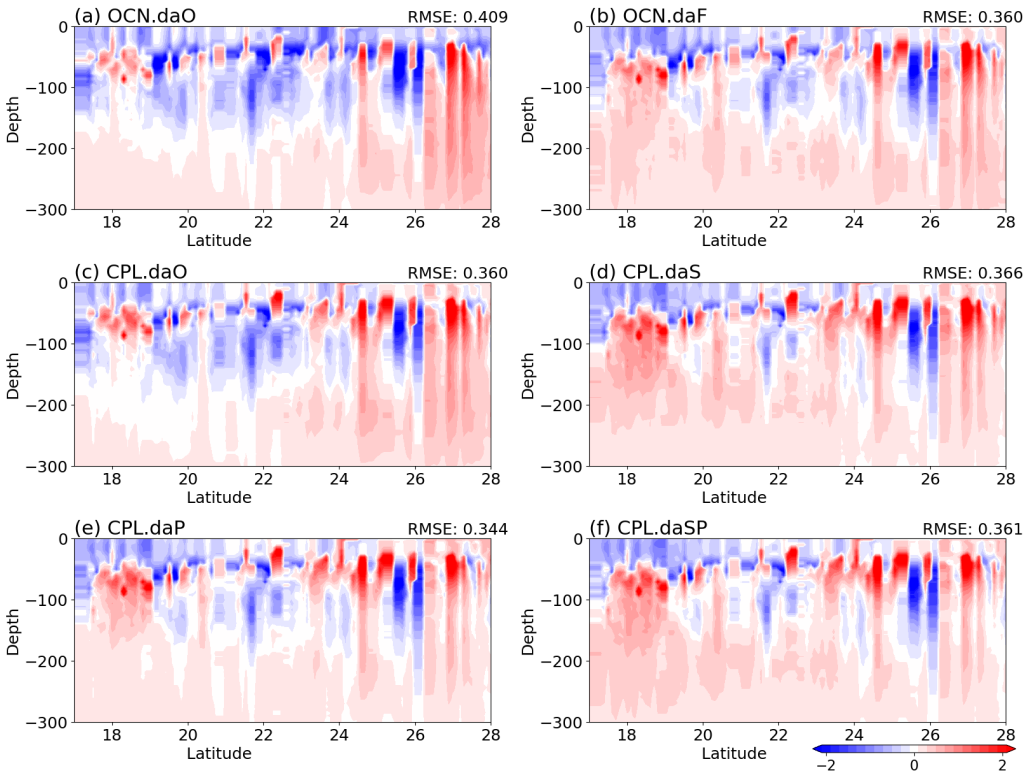

Figure 9. The differences between the temperature at 0-300 m obtained in the DA experiments compared to in situ observations (results minus observations).

Bannister, R. N. (2008a). A review of forecast error covariance statistics in atmospheric variational data assimilation. I: Characteristics and measurements of forecast error covariances. *Quarterly Journal of the Royal Meteorological Society*, *134*(637, B), 1951-1970. doi: 10.1002/qj.339

Bannister, R. N. (2008b). A review of forecast error covariance statistics in atmospheric variational data assimilation. II: Modelling the forecast error covariance statistics. *Quarterly Journal of the Royal Meteorological Society*, *134*(637), 1971-1996. doi: 10.1002/qj.340

Bannister, R. N. (2017). A review of operational methods of variational and ensemble-variational data assimilation. *Quarterly Journal of the Royal Meteorological Society*, *143*(703), 607–633.

Banzon, V., Smith, T. M., Chin, T. M., Liu, C., & Hankins, W. (2016). A long-term record of blended satellite and in situ sea-surface temperature for climate monitoring, modeling and environmental studies. *Earth System Science Data*, *8*(1), 165–176.

Berner, J., Fossell, K., Ha, S.-Y., Hacker, J., & Snyder, C. (2015). Increasing the skill of probabilistic forecasts: Understanding performance improvements from model-error representations. *Monthly Weather Review*, *143*(4), 1295–1320.

Berner, J., Ha, S.-Y., Hacker, J., Fournier, A., & Snyder, C. (2011). Model uncertainty in a mesoscale ensemble prediction system: Stochastic versus multiphysics representations. *Monthly Weather Review*, *139*(6), 1972–1995.

Berner, J., Shutts, G., Leutbecher, M., & Palmer, T. (2009). A spectral stochastic kinetic energy backscatter scheme and its impact on flow-dependent predictability in the ECMWF ensemble prediction system. *Journal of the Atmospheric Sciences*, *66*(3), 603–626.

Bougeault, P., Toth, Z., Bishop, C., Brown, B., Burridge, D., Chen, D. H., ... others (2010). The THORPEX interactive grand global ensemble. *Bulletin of the*

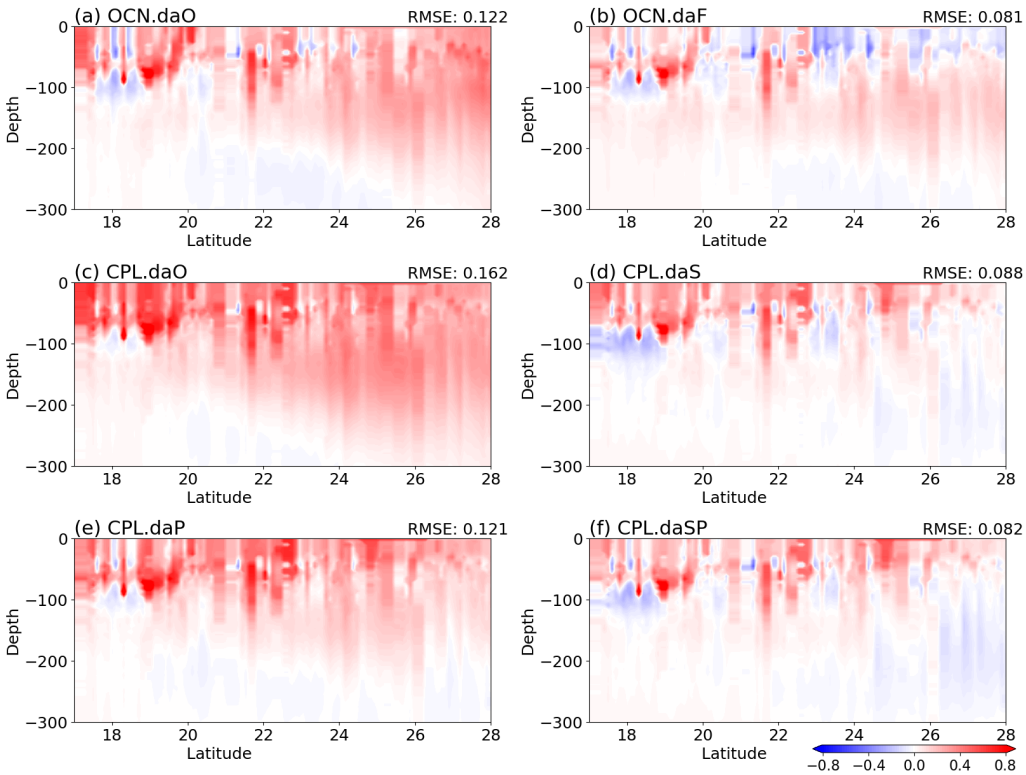

Figure 10. The differences between the salinity at 0-300 m obtained in the DA experiments in comparison with in situ observations (results minus observations).

American Meteorological Society, *91*(8), 1059–1072.

Brankart, J.-M., Candille, G., Garnier, F., Calone, C., Melet, A., Bouttier, P.-A., ... Verron, J. (2015). A generic approach to explicit simulation of uncertainty in the NEMO ocean model. *Geoscientific Model Development*, *8*(5), 1285-1297. doi: 10.5194/gmd-8-1285-2015

Buizza, R. (2014). *The TIGGE global, medium-range ensembles.* European Centre for Medium-Range Weather Forecasts.

Campin, J.-M., Heimbach, P., Losch, M., Forget, G., edhill3, Adcroft, A., ... T., A. T. (2019). Mitgcm/mitgcm: checkpoint67m. doi: 10.5281/zenodo.3492298

Chen, S.-H., & Sun, W.-Y. (2002). A one-dimensional time dependent cloud model. *Journal of the Meteorological Society of Japan. Ser. II*, *80*(1), 99–118.

Cox, M. (1987). Isopycnal diffusion in a z-coordinate ocean model. *Ocean modelling*, *74*, 1–5.

Danabasoglu, G., & McWilliams, J. (1995). Sensitivity of the global ocean circulation to parameterizations of mesoscale tracer transports. *Journal of Climate*, *8*(12), 2967-2987. doi: 10.1175/1520-0442(1995)008⟨2967:SOTGOC⟩2.0.CO;2

Dasari, H. P., Desamsetti, S., Langodan, S., Attada, R., Ashok, K., & Hoteit, I. (n.d.). Long-term changes in the Arabian Peninsula rainfall and their relationship with the ENSO signals in the tropical Indo-Pacific. *Climate Dynamics*, 1–17.

Davis, S. R., Farrar, J. T., Weller, R. A., Jiang, H., & Pratt, L. J. (2019). The land-sea breeze of the Red Sea: observations, simulations, and relationships to regional moisture transport. *Journal of Geophysical Research: Atmospheres*, *124*(24), 13803–13825.

Donlon, C. J., Martin, M., Stark, J., Roberts-Jones, J., Fiedler, E., & Wimmer, W. (2012). The operational sea surface temperature and sea ice analysis (OSTIA)

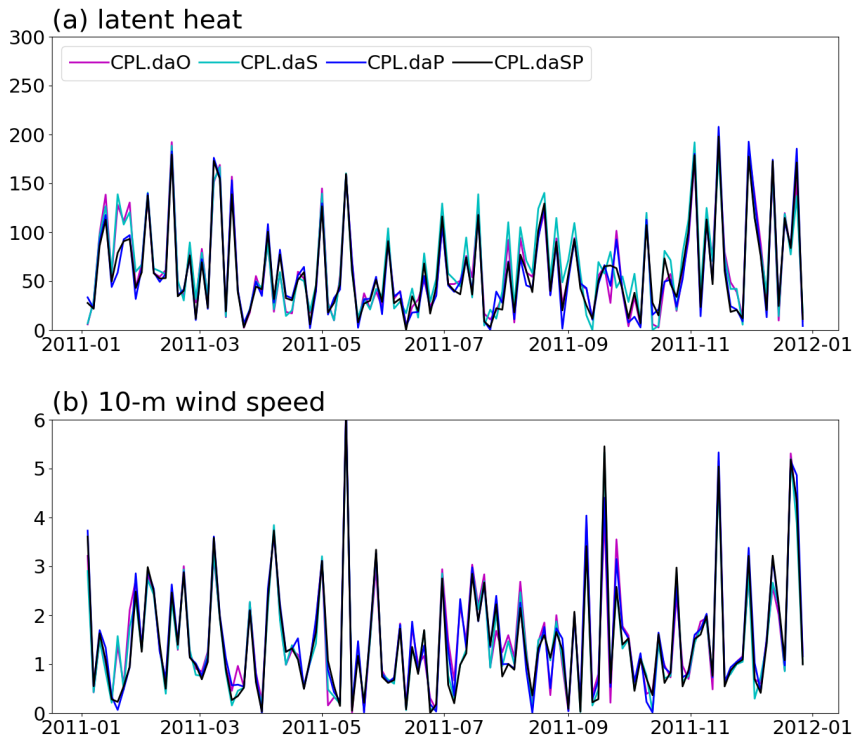

Figure 11. The RMSEs of latent heat flux and 10-m wind speed obtained in the coupled model when assimilating the ocean data. We only compare the data on the centerline of the Red Sea.

system. *Remote Sensing of Environment*, *116*, 140–158.

Edwards, C. A., Moore, A. M., Hoteit, I., & Cornuelle, B. D. (2015). Regional ocean data assimilation. In C. Carlson & S. Giovannoni (Eds.), *Annual review of marine science, vol 7* (Vol. 7, p. 21-42). doi: 10.1146/annurev-marine-010814-015821

Evensen, G. (1994). Sequential data assimilation with a nonlinear quasi-geostrophic model using Monte Carlo methods to forecast error statistics. *Journal of Geophysical Research: Oceans*, *99*(C5), 10143–10162.

Evensen, G. (2003). The ensemble Kalman filter: Theoretical formulation and practical implementation. *Ocean dynamics*, *53*, 343–367.

Evensen, G. (2004). Sampling strategies and square root analysis schemes for the enkf. *Ocean Dynamics*, *54*(6), 539-560. doi: 10.1007/s10236-004-0099-2

Evensen, G., & Van Leeuwen, P. J. (1996). Assimilation of Geosat altimeter data for the Agulhas current using the ensemble Kalman filter with a quasigeostrophic model. *Monthly Weather Review*, *124*(1), 85–96.

Fairall, C., Bradley, E. F., Hare, J., Grachev, A., & Edson, J. (2003). Bulk parameterization of air–sea fluxes: Updates and verification for the COARE algorithm. *Journal of Climate*, *16*(4), 571–591.

Gaspar, P., Gregoris, Y., & Lefevre, J. (1990). A simple eddy kinetic-energy model for simulations of the oceanic vertical mixing - Tests at station Papa and long-term upper ocean study site. *Journal of Geophysical Research-Oceans*, *95*(C9), 16179-16193. doi: 10.1029/JC095iC09p16179

Gent, P., & Mcwilliams, J. (1990). Isopycnal mixing in ocean circulation models. *Journal of Physical Oceanography*, *20*(1), 150-155. doi: 10.1175/1520-0485(1990)020⟨0150:IMIOCM⟩2.0.CO;2

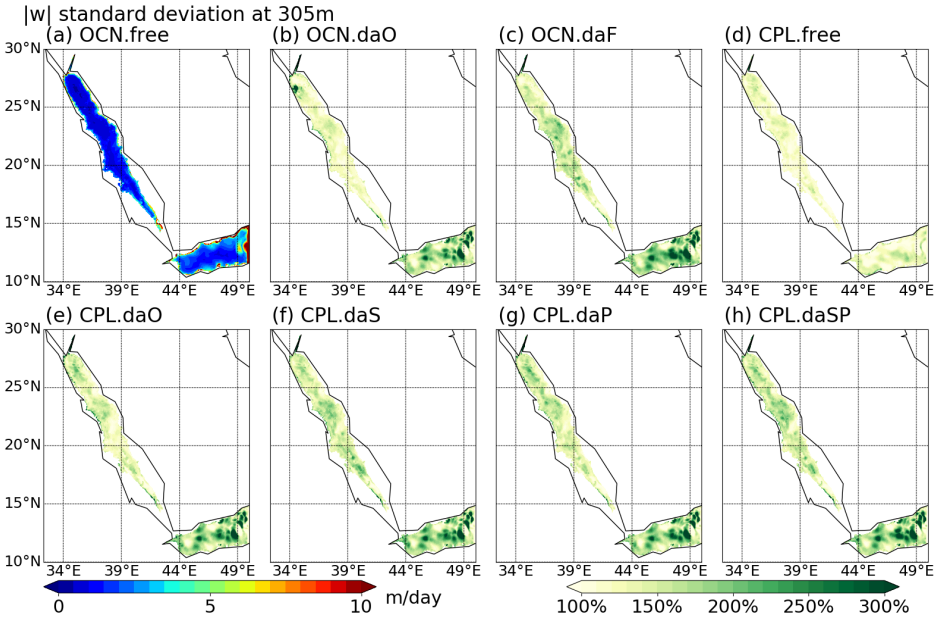

Figure 12. Standard deviation of $|w|$ at 300 m obtained in the DA experiments. Panels (b)-(h) are normalized by the reference OCN.free in panel (a) to highlight differences.

Gent, P., Willebrand, J., Mcdougall, T., & Mcwilliams, J. (1995). Parameterizing eddy-induced tracer transports in ocean circulation models. *Journal of Physical Oceanography*, *25*(4), 463-474. doi: 10.1175/1520-0485(1995)025⟨0463:PEITTI⟩2.0.CO;2

Good, S. A., Martin, M. J., & Rayner, N. A. (2013). EN4: Quality controlled ocean temperature and salinity profiles and monthly objective analyses with uncertainty estimates. *Journal of Geophysical Research: Oceans*, *118*(12), 6704–6716.

Grell, G. A., & Freitas, S. R. (2014). A scale and aerosol aware stochastic convective parameterization for weather and air quality modeling. *Atmospheric Chemistry and Physics*, *14*(10), 5233–5250.

Griffies, S., & Hallberg, R. (2000). Biharmonic friction with a smagorinsky-like viscosity for use in large-scale eddy-permitting ocean models. *Monthly Weather Review*, *128*(8, 2), 2935-2946. doi: 10.1175/1520-0493(2000)128⟨2935:BFWASL⟩2.0.CO;2

Harrop, C., samtrahan, christinaholt, & Brown, T. (2017, Sep). christopherwharrop/rocoto: Rocoto 1.2.4. doi: 10.5281/zenodo.890939

Hill, C., DeLuca, C., Balaji, Suarez, M., & Silva, A. (2004). The architecture of the earth system modeling framework. *Computing in Science & Engineering*, *6*(1), 18–28.

Holland, W. (1978). Role of mesoscale eddies in general circulation of ocean - numerical experiments using a wind-driven quasi-geostrophic model. *Journal of Physical Oceanography*, *8*(3), 363-392. doi: 10.1175/1520-0485(1978)008⟨0363:TROMEI⟩2.0.CO;2

Hong, S.-Y., & Lim, J.-O. J. (2006). The WRF single-moment 6-class microphysics scheme (WSM6). *Asia-Pacific Journal of Atmospheric Sciences*, *42*(2), 129–151.

Hong, S.-Y., Noh, Y., & Dudhia, J. (2006). A new vertical diffusion package with an explicit treatment of entrainment processes. *Monthly Weather Review*, *134*(9), 2318–2341.

Hoteit, I., Abualnaja, Y., Afzal, S., Ait-El-Fquih, B., Akylas, T., Antony, C., ... Zodiatis, G. (2021). Towards an end-to-end analysis and prediction system for weather, climate, and marine applications in the Red Sea. *Bulletin of the American Meteorological Society*, *102*(1), E99 - E122. Retrieved from `https://journals.ametsoc.org/view/journals/bams/102/1/BAMS-D-19-0005.1.xml` doi: https://doi.org/10.1175/BAMS-D-19-0005.1

Hoteit, I., Cornuelle, B., & Heimbach, P. (2010). An eddy-permitting, dynamically consistent adjoint-based assimilation system for the tropical Pacific: Hindcast experiments in 2000. *Journal of Geophysical Research: Oceans*, *115*(C3).

Hoteit, I., Hoar, T., Gopalakrishnan, G., Collins, N., Anderson, J., Cornuelle, B., ... Heimbach, P. (2013). A MITgcm/DART ensemble analysis and prediction system with application to the Gulf of Mexico. *Dynamics of Atmospheres and Oceans*, *63*, 1–23.

Hoteit, I., Pham, D., & Blum, J. (2002). A simplified reduced order Kalman filtering and application to altimetric data assimilation in Tropical Pacific. *Journal of Marine Systems*, *36*(1-2), 101-127. doi: 10.1016/S0924-7963(02)00129-X

Hoteit, I., Pham, D.-T., Gharamti, M., & Luo, X. (2015). Mitigating observation perturbation sampling errors in the stochastic EnKF. *Monthly Weather Review*, *143*(7), 2918–2936.

Houtekamer, P. L., Mitchell, H. L., Pellerin, G., Buehner, M., Charron, M., Spacek, L., & Hansen, B. (2005). Atmospheric data assimilation with an ensemble Kalman filter: Results with real observations. *Monthly Weather Review*, *133*(3), 604–620.

Iacono, M. J., Delamere, J. S., Mlawer, E. J., Shephard, M. W., Clough, S. A., & Collins, W. D. (2008). Radiative forcing by long-lived greenhouse gases: Calculations with the AER radiative transfer models. *Journal of Geophysical Research: Atmospheres*, *113*(D13).

Ingleby, B., & Huddleston, M. (2007). Quality control of ocean temperature and salinity profiles—Historical and real-time data. *Journal of Marine Systems*, *65*(1-4), 158–175.

Janjić, Z. I. (1994). The step-mountain eta coordinate model: Further developments of the convection, viscous sublayer, and turbulence closure schemes. *Monthly Weather Review*, *122*(5), 927–945.

Jean-Michel, L., Eric, G., Romain, B.-B., Gilles, G., Angélique, M., Marie, D., ... others (2021). The Copernicus global 1/12 oceanic and sea ice GLORYS12 reanalysis. *Frontiers in Earth Science*, *9*, 698876.

Kain, J. S. (2004). The kain–fritsch convective parameterization: an update. *Journal of applied meteorology*, *43*(1), 170–181.

Karspeck, A. R., Yeager, S., Danabasoglu, G., Hoar, T., Collins, N., Raeder, K., ... Tribbia, J. (2013). An ensemble adjustment Kalman filter for the CCSM4 ocean component. *Journal of Climate*, *26*(19), 7392-7413. doi: 10.1175/JCLI-D-12-00402.1

Kwon, K. M., Choi, B.-J., Lee, S.-H., Kim, Y. H., Seo, G.-H., & Cho, Y.-K. (2016). Effect of model error representation in the Yellow and East China Sea modeling system based on the ensemble Kalman filter. *Ocean Dynamics*, *66*(2), 263-283. doi: 10.1007/s10236-015-0909-8

Kwon, Y. C., & Hong, S.-Y. (2017). A mass-flux cumulus parameterization scheme across gray-zone resolutions. *Monthly Weather Review*, *145*(2), 583–598.

Langodan, S., Cavaleri, L., Vishwanadhapalli, Y., Pomaro, A., Bertotti, L., & Hoteit, I. (2017). The climatology of the Red Sea–part 1: the wind. *International Journal of Climatology*, *37*(13), 4509–4517.

Large, W., Danabasoglu, G., Doney, S., & McWilliams, J. (1997). Sensitivity to surface forcing and boundary layer mixing in a global ocean model: Annual-mean climatology. *Journal of Physical Oceanography*, *27*(11), 2418-2447. doi: 10.1175/1520-0485(1997)027⟨2418:STSFAB⟩2.0.CO;2

Large, W. G., McWilliams, J. C., & Doney, S. C. (1994). Oceanic vertical mixing: A review and a model with a nonlocal boundary layer parameterization. *Reviews of Geophysics*, *32*(4), 363–403.

Lawson, W., & Hansen, J. (2004). Implications of stochastic and deterministic filters as ensemble-based data assimilation methods in varying regimes of error growth. *Monthly Weather Review*, *132*(8), 1966-1981. doi: 10.1175/1520-0493(2004)132⟨1966:IOSADF⟩2.0.CO;2

Leeuwenburgh, O., Evensen, G., & Bertino, L. (2005). The impact of ensemble filter definition on the assimilation of temperature profiles in the tropical Pacific. *Quarterly Journal of the Royal Meteorological Society*, *131*(613, C), 3291-3300. doi: 10.1256/qj.05.90

Leith, C. (1996). Stochastic models of chaotic systems. *PHYSICA D*, *98*(2-4), 481-491. (15th Annual International Conference of the Center-for-Nonlinear-Studies on Nonlinear Phenomena in Ocean Dynamics, LOS ALAMOS, NM, MAY 15-19, 1995) doi: 10.1016/0167-2789(96)00107-8

Lim, K.-S. S., & Hong, S.-Y. (2010). Development of an effective double-moment cloud microphysics scheme with prognostic cloud condensation nuclei (CCN) for weather and climate models. *Monthly Weather Review*, *138*(5), 1587–1612.

Lima, L. N., Pezzi, L. P., Penny, S. G., & Tanajura, C. A. S. (2019). An investigation of ocean model uncertainties through ensemble forecast experiments in the southwest Atlantic Ocean. *Journal of Geophysical Research-Oceans*, *124*(1), 432-452. doi: 10.1029/2018JC013919

Lisæter, K. A., Rosanova, J., & Evensen, G. (2003). Assimilation of ice concentration in a coupled ice–ocean model, using the ensemble Kalman filter. *Ocean Dynamics*, *53*(4), 368–388.

Liu, P., Tsimpidi, A., Hu, Y., Stone, B., Russell, A., & Nenes, A. (2012). Differences between downscaling with spectral and grid nudging using WRF. *Atmospheric Chemistry and Physics*, *12*(8), 3601–3610.

Luo, X., & Hoteit, I. (2012). Ensemble Kalman filtering with residual nudging. *Tellus A: Dynamic Meteorology and Oceanography*, *64*(1), 17130.

Marshall, J., Adcroft, A., Hill, C., Perelman, L., & Heisey, C. (1997). A finite-volume, incompressible Navier Stokes model for studies of the ocean on parallel computers. *Journal of Geophysical Research: Oceans*, *102*(C3), 5753–5766.

Mellor, G., & Yamada, T. (1982). Development of a turbulence closure-model for geophysical fluid problems. *Reviews of Geophysics*, *20*(4), 851-875. doi: 10.1029/RG020i004p00851

Mertz, F., Rosmorduc, V., Maheu, C., & Faugére, Y. (2017). *Product user manual, For sea level SLA products.*

Morrison, H., Thompson, G., & Tatarskii, V. (2009). Impact of cloud microphysics on the development of trailing stratiform precipitation in a simulated squall line: Comparison of one-and two-moment schemes. *Monthly Weather Review*, *137*(3), 991–1007.

Nakanishi, M., & Niino, H. (2004). An improved Mellor–Yamada level-3 model with condensation physics: Its design and verification. *Boundary-Layer Meteorology*, *112*(1), 1–31.

Nakanishi, M., & Niino, H. (2009). Development of an improved turbulence closure model for the atmospheric boundary layer. *Journal of the Meteorological Society of Japan. Ser. II*, *87*(5), 895–912.

Oakley, N. S., Liu, T., McGuire, L. A., Simpson, M., Hatchett, B. J., Tardy, A., ... Steinhoff, D. (2023). Toward probabilistic post-fire debris-flow hazard decision support. *Bulletin of the American Meteorological Society*.

Pacanowski, R., & Philander, S. (1981). Parameterization of vertical mixing in numerical models of tropical oceans. *Journal of Physical Oceanography*, *11*(11), 1443–1451.

Park, J.-Y., Stock, C. A., Yang, X., Dunne, J. P., Rosati, A., John, J., & Zhang, S. (2018). Modeling global ocean biogeochemistry with physical data assimilation: a pragmatic solution to the equatorial instability. *Journal of Advances in Modeling Earth Systems*, *10*(3), 891–906.

Penny, S. G., Behringer, D. W., Carton, J. A., & Kalnay, E. (2015). A hybrid global ocean data assimilation system at NCEP. *Monthly Weather Review*, *143*(11), 4660-4677. doi: 10.1175/MWR-D-14-00376.1

Prakash, P. J., Stenchikov, G., Kalenderski, S., Osipov, S., & Bangalath, H. (2014). The impact of dust storms on the Arabian Peninsula and the Red Sea. *Atmospheric Chemistry & Physics Discussions*, *14*(13).

Redi, M. (1982). Oceanic isopycnal mixing by coordinate rotation. *Journal of Physical Oceanography*, *12*(10), 1154-1158. doi: 10.1175/1520-0485(1982)012⟨1154:OIMBCR⟩2.0.CO;2

Reynolds, R. W., Smith, T. M., Liu, C., Chelton, D. B., Casey, K. S., & Schlax, M. G. (2007). Daily high-resolution-blended analyses for sea surface temperature. *Journal of climate*, *20*(22), 5473–5496.

Sakov, P., Counillon, F., Bertino, L., Lisæter, K., Oke, P., & Korablev, A. (2012). Topaz4: an ocean-sea ice data assimilation system for the North Atlantic and Arctic. *Ocean Science*, *8*(4), 633–656.

Sandery, P. A., Sakov, P., & Majewski, L. (2014). The impact of open boundary forcing on forecasting the east australian current using ensemble data assimilation. *Ocean Modelling*, *84*, 1-11. doi: 10.1016/j.ocemod.2014.09.005

Sanikommu, S., Banerjee, D. S., Baduru, B., Paul, B., Paul, A., Chakraborty, K., & Hoteit, I. (2019). Impact of dynamical representational errors on an indian ocean ensemble data assimilation system. *Quarterly Journal of the Royal Meteorological Society*, *145*(725), 3680–3691.

Sanikommu, S., Langodan, S., Dasari, H. P., Zhan, P., Krokos, G., Abualnaja, Y. O., ... Hoteit, I. (2023a). Making the case for high resolution regional ocean reanalyses: An example with the Red Sea. *Bulletin of the American Meteorological Society*, E1241–E1264.

Sanikommu, S., Langodan, S., Dasari, H. P., Zhan, P., Krokos, G., Abualnaja, Y. O., ... Hoteit, I. (2023b). Making the case for high-resolution regional ocean reanalyses: An example with the Red Sea. *Bulletin of the American Meteorological Society*, *104*(7), E1241 - E1264. Retrieved from `https://journals.ametsoc.org/view/journals/bams/104/7/BAMS-D-21-0287.1.xml` doi: https://doi.org/10.1175/BAMS-D-21-0287.1

Sanikommu, S., Paul, A., Sluka, T., Ravichandran, M., & Kalnay, E. (2017). The pre-argo ocean reanalyses may be seriously affected by the spatial coverage of moored buoys. *SCIENTIFIC REPORTS*, *7*. doi: 10.1038/srep46685

Sanikommu, S., Toye, H., Zhan, P., Langodan, S., Krokos, G., Knio, O., & Hoteit, I. (2020). Impact of atmospheric and model physics perturbations on a high-resolution ensemble data assimilation system of the Red Sea. *Journal of Geophysical Research: Oceans*, *125*(8), e2019JC015611.

Shu, Y., Zhu, J., Wang, D., & Xiao, X. (2011). Assimilating remote sensing and in situ observations into a coastal model of northern South China Sea using ensemble Kalman filter. *Continental Shelf Research*, *31*(6, S, SI), S24-S36. doi: 10.1016/j.csr.2011.01.017

Shutts, G. (2005). A kinetic energy backscatter algorithm for use in ensemble prediction systems. *Quarterly Journal of the Royal Meteorological Society: A journal of the atmospheric sciences, applied meteorology and physical oceanography*, *131*(612), 3079–3102.

Skamarock, W. C., Klemp, J. B., Dudhia, J., Gill, D. O., Liu, Z., Berner, J., ... others (2019). A description of the advanced research WRF model version 4. *National Center for Atmospheric Research: Boulder, CO, USA*, *145*(145), 550.

Smagorinsky, J., Galperin, B., & Orszag, S. (1993). Large eddy simulation of complex engineering and geophysical flows. *Evolution of physical oceanography*, 3–36.

Song, H., Hoteit, I., Cornuelle, B. D., & Subramanian, A. C. (2010). An adaptive approach to mitigate background covariance limitations in the ensemble Kalman filter. *Monthly Weather Review*, *138*(7), 2825–2845.

Stark, J. D., Donlon, C. J., Martin, M. J., & McCulloch, M. E. (2007). OSTIA: An operational, high resolution, real time, global sea surface temperature analysis system. In *Oceans 2007-europe* (pp. 1–4).

Sun, R., Cobb, A., Villas Bôas, A. B., Langodan, S., Subramanian, A. C., Mazloff, M. R., ... Hoteit, I. (2023). Waves in SKRIPS: WAVEWATCH III coupling implementation and a case study of tropical cyclone mekunu. *Geoscientific Model Development*, *16*(12), 3435–3458.

Sun, R., Subramanian, A. C., Miller, A. J., Mazloff, M. R., Hoteit, I., & Cornuelle, B. D. (2019). SKRIPS v1.0: a regional coupled ocean–atmosphere modeling framework (MITgcm–WRF) using ESMF/NUOPC, description and preliminary results for the Red Sea. *Geoscientific Model Development*, *12*(10), 4221–4244. doi: 10.5194/gmd-12-4221-2019

Tewari, M., Chen, F., Wang, W., Dudhia, J., LeMone, M., Mitchell, K., ... Cuenca, R. (2004). Implementation and verification of the unified NOAH land surface model in the WRF model. In *20th conference on weather analysis and forecasting/16th conference on numerical weather prediction* (Vol. 1115).

Thompson, G., Field, P. R., Rasmussen, R. M., & Hall, W. D. (2008). Explicit forecasts of winter precipitation using an improved bulk microphysics scheme. Part II: Implementation of a new snow parameterization. *Monthly Weather Review*, *136*(12), 5095–5115.

Toye, H., Zhan, P., Gopalakrishnan, G., Kartadikaria, A. R., Huang, H., Knio, O., & Hoteit, I. (2017). Ensemble data assimilation in the Red Sea: sensitivity to ensemble selection and atmospheric forcing. *Ocean Dynamics*, *67*(7), 915-933. doi: 10.1007/s10236-017-1064-1

Vandenbulcke, L., & Barth, A. (2015). A stochastic operational forecasting system of the Black Sea: Technique and validation. *Ocean Modelling*, *93*, 7-21. doi: 10.1016/j.ocemod.2015.07.010

Wan, L., Zhu, J., Bertino, L., & Wang, H. (2008). Initial ensemble generation and validation for ocean data assimilation using HYCOM in the Pacific. *Ocean Dynamics*, *58*, 81–99.

Whitaker, J. S., & Hamill, T. M. (2012). Evaluating methods to account for system errors in ensemble data assimilation. *Monthly Weather Review*, *140*(9), 3078-3089. doi: 10.1175/MWR-D-11-00276.1

Zhai, P., Bower, A. S., Smethie Jr, W. M., & Pratt, L. J. (2015). Formation and spreading of Red Sea outflow water in the Red Sea. *Journal of Geophysical Research: Oceans*, *120*(9), 6542–6563.

Zhang, C., & Wang, Y. (2017). Projected future changes of tropical cyclone activity over the western North and South Pacific in a 20-km-mesh regional climate model. *Journal of Climate*, *30*(15), 5923–5941.

Zhang, F., Snyder, C., & Sun, J. (2004). Impacts of initial estimate and observation availability on convective-scale data assimilation with an ensemble Kalman filter. *Monthly Weather Review*, *132*(5), 1238-1253. doi: 10.1175/1520-0493(2004)132⟨1238:IOIEAO⟩2.0.CO;2